Carboxymethyl Chitosan Aerogels Reinforced with TEMPO-oxidized Cellulose Nanofibers for Efficient Adsorption of Pb(II) Ions in Aqueous Media

Na Young Kang,^a Soon Wan Kweon ^[D],^a Jin Ho Seo,^b Tai Ju Lee,^{a,*} and Hyoung Jin Kim ^{a,*}

A reinforced composite aerogel composed of carboxymethyl chitosan (CMCS) and cellulose nanofibers (CNFs) was synthesized via chemical crosslinking with epichlorohydrin (EH) for the efficient removal of Pb(II) ions from aqueous solutions. The CMCS, a chitosan derivative, was successfully prepared through a simple chemical reaction with a degree of substitution of 1.96. The incorporation of CNFs imparted enhanced mechanical stability to the aerogel matrix and increased the surface area, whereas carboxymethyl cellulose contributed functional carboxyl groups that facilitated efficient metal ion adsorption. In addition, crosslinking with EH significantly improved the structural integrity and water stability of the aerogels, rendering them suitable for application in aqueous environments. The composite aerogels exhibited a porous structure and good adsorption of lead ions (Pb2+) in water with a removal percentage of 98%. Upon the addition of 1 wt% CNF loading, the compression strength of the composite aerogels was enhanced 42% compared with the samples without CNF loading. The adsorption kinetics showed a high correlation with the pseudo-second-order model (R² = 0.99). The good structural stability and water absorption of the prepared CMCS aerogels make them an ideal candidate for eco-friendly heavy metal-ion treatment.

DOI: 10.15376/biores.20.4.10618-10639

Keywords: Carboxymethyl chitosan; Aerogel; Heavy metal ions; Adsorbent; Epichlorohydrin; Cellulose nanofiber (CNF); Adsorption kinetics

Contact information: a: Department of Forest Products and Biotechnology, Kookmin University, 77 Jeongneung-ro, Seongbuk-gu, Seoul 02707 Republic of Korea; b: Department of Paper Material Science and Engineering, Kangwon National University, 1 Kangwondaehak-gil, Chuncheon-si, Gangwon-do 24341 Republic of Korea;

 $*\ Corresponding\ authors:\ leetj@kookmin.ac.kr,\ hyjikim@kookmin.ac.kr$

INTRODUCTION

Heavy metals are metallic elements with a high density of 4.5 or more that exhibit toxicity or harmful effects when they are in an ionic form even at low concentrations (Duruibe *et al.* 2007). Common heavy metals include lead (Pb), zinc (Zn), mercury, nickel, cadmium (Cd), copper (Cu), chromium (Cr), and arsenic (As). Countries around the world strictly regulate the permissible discharge standards for heavy metals in their effluent standards for water pollutants because heavy metals have adverse effects on the human kidneys and nervous system (Yu *et al.* 2019). The concentration of Pb ions in industrial wastewater is 200 to 500 mg/L, which is significantly higher than the water quality standards and must be reduced to 0.1 to 0.05 mg/L (Özacar *et al.* 2008). Therefore, an appropriate method for removing heavy metals from sewage is required. Common methods for removing heavy metal ions from wastewater include flotation, ion exchange, coagulation/flocculation, adsorption, and extraction (Shrestha *et al.* 2021). Adsorption methods, particularly with the use of aerogels, are extensively used in environmentally friendly treatment processes because of their high removal efficiency, low cost, economic feasibility, and simple and

convenient operation. The main types of aerogels are carbon-based aerogels (Goel *et al.* 2005), mineral-based aerogels (Zhao *et al.* 2023), synthetic polymer-based aerogels (Mo *et al.* 2022), and natural polymer-based aerogels (Bekchanov *et al.* 2024). Green aerogel absorbents based on natural polymers, such as cellulose, alginate, starch, chitosan, and cyclodextrin, are cost-effective, biodegradable, and renewable, making them environmentally friendly. They also exhibit good heavy metal-ion adsorption ability because of their physicochemical properties, high reactivity with ionic pollutants, and active functional groups such as OH, NH₂, NHCOOCH₃, and COO⁻ (Abdel-Halim and Al-Deyab 2011).

Chitosan is a deacetylated derivative of chitin that is obtained from the shells of crabs and shrimp and is one of the most abundant biopolymers after cellulose (Gu et al. 2019). Because of the protonation of its NH₂ groups in acidic media, and NH₂ and OH groups from hydrogen bonds that form either intermolecularly or intramolecularly, chitosan dissolves in weak acid solvents and forms a rigid crystalline structure (Rinaudo et al. 1999). In addition, various chemical functional groups exhibit strong adsorption capacity for ionic heavy metal pollutants (Erosa et al. 2001). Li (2016) fabricated chitosan aerogels by freeze-drying, yielding aerogels with low density (0.0283 g/cm³), high porosity (98.0%), and excellent Cu-ion adsorption capacity (35.1 mg/g). Despite its strong adsorption capacity, chitosan has a drawback in that it dissolves only in acidic solutions at specific pH levels because of the protonation of its amine groups (R-NH⁺3) (Sorlier et al. 2001).

To improve the solubility of chitosan, various chemical modifications have been applied. Among these modifications, carboxymethyl chitosan (CMCS) is a representative water-soluble chitosan derivative produced by reacting with monochloroacetic acid (MCA) in an alkaline medium. CMCS contains various functional groups such as COOH, OH, and NH2 (Chen *et al.* 2003). Three types of CMCS can be produced, depending on where the carboxyl group is synthesized. Carboxymethylation of chitosan in the amine group yields N-CMCS, whereas modification in the hydroxyl group results in O-CMCS. Simultaneous modification at both sites leads to the formation of N,O-CMCS (Zając *et al.* 2023). Amphiprotic O-CMCS contains both carboxyl and amine groups, conferring high solubility and pH-responsive surface charge characteristics across a wide pH range. These characteristics broaden the solubility range of CMCS in both acidic and alkaline media, thereby facilitating the selective adsorption of ionic contaminants (Sun *et al.* 2006; Wu *et al.* 2010; Borsagli *et al.* 2015).

Despite the incontrovertible advantages of O-CMCS as a raw adsorbent material, it is difficult to use alone because of the collapse of its structure after swelling in aqueous media. To solve this problem, crosslinking is essential for ensuring the structural integrity and functional performance of CMCS-based aerogels (Bhattarai et al. 2010). Common chemical crosslinkers for chitosan and CMCS include glutaraldehyde, epichlorohydrin (EH), ethylene glycol (Ngah et al. 2005), and tripolyphosphate (Mi et al. 1999). However, glutaraldehyde or dialdehyde preferentially combines with amine and hydroxyl groups, thereby decreasing the number of active sites and inhibiting the adsorption capacity (Jawad et al. 2019). EH is a base-catalyzed crosslinking agent that exhibits low reactivity with amine groups and primarily binds with hydroxyl groups (Jawad et al. 2012). Thus, EH not only preserves the structural stability of CMCS-based aerogels obtained by freeze-drying, but it also prevents a reduction in the number of active sites during adsorption. Although chemical crosslinking provides stronger network interactions than physical crosslinking, the mechanical strength of chemically crosslinked porous aerogels is insufficient, indicating the need for further research on the incorporation of nanofillers as reinforcing agents.

To address the limitations of natural polymer-based aerogels, such as insufficient mechanical strength, shrinkage, and deformation during drying, nanofillers have been introduced as effective reinforcing agents (Esmaeili *et al.* 2021). Cellulose nanofibers (CNFs), which are the nanofillers, have been extensively explored because of their distinctive properties, such as biodegradability, large surface area, high crystallinity, high aspect ratio, and low density (Yano *et al.* 2018).

In this context, the combination of CMCS and TEMPO-oxidized CNFs was chosen to achieve a synergistic effect. CMCS offers abundant carboxyl groups that provide strong binding sites for Pb²⁺ ions, while CNFs contribute a high surface area and a reinforcing nanofibrous network that enhances the structural stability of the aerogels. This dual functionality is expected to ensure both high adsorption capacity and mechanical integrity, which are critical for practical applications.

Accordingly, in the present study, O-CMCS was synthesized *via* carboxy-methylation, and environmentally friendly aerogels were prepared through a freezedrying process. The effects of EH-induced crosslinking and CNF incorporation on the physicochemical properties, mechanical strength, and Pb²⁺ adsorption performance of O-CMCS-based aerogels were systematically investigated, with particular emphasis on adsorption kinetics.

EXPERIMENTAL

Materials

Chitosan (Mw: 190 to 375 KDa, deacetylation degree: 85%, particle size: 425 to 850 μ m) was obtained from Sigma-Aldrich (Shanghai, China). EH (99.5%) was purchased from Junsei (Tokyo, Japan). CNFs oxidized with TEMPO (2,2,6,6-tetramethylpiperidin-1-oxyl radical) (T-CNFs, 2 wt%, ANPOLY, South Korea) were used as nanofillers. The characteristics of T-CNFs are presented in Table 1.

The solution used to synthesize CMCS contained isopropanol alcohol (IPA, Daejung, Korea, 97%), sodium hydroxide (NaOH, Deajung, Korea, 97%), MCA (Duksan, Korea), and acetic acid (Daejung, Korea).

Table	1 F	Properties	of T	CNFs
Iabic		100011103	OI I	-CIVI 3

Carboxylate Content (mmol/g)	рН	Conductivity (mS/cm)	Zeta Potential (mV)	Fiber Width (nm)	Fiber Length (nm)
1.6 to 1.85	6 to 8	< 1.5	- 56.1 ± 8.4	6.12 ± 3.67	1852 ± 1269

Synthesis of CMCS

The CMCS synthesis method was described in a previous study (Chen *et al.* 2003). The reaction conditions are summarized in Table 2. Chitosan was mixed with an isopropyl alcohol (IPA) solution, to which NaOH dissolved in distilled water was added. The reaction was conducted for 1 h. Subsequently, MCA dissolved in IPA was slowly added dropwise to the chitosan solution and reacted for 4 h according to the temperature conditions. After stirring, 70% ethyl alcohol was added to stop the reaction, and the solution was then neutralized to pH 7 using acetic acid. The purification process was performed three times using 70% and, 90% ethyl alcohol. After drying in an oven at 40 °C, CMCS powder was obtained.

Sample code	Temperature (°C)	Chitosan (g)	MCA (g)	IPA (mL)	70% EtOH (mL)	NaOH (mmol/g)
CMCS RT	Room Temperature					
CMCS 30	30		4 =	50	00	40.07
CMCS 40	40	3	4.5	50	60	10.07
CMCS 50	50					
CMCS 60	60					

Table 2. Reaction Conditions for Carboxymethylation of Chitosan

Determination of Degree of Substitution (DS)

The substitutions of carboxyl groups at the C₆, C₃, and C₂-NH₂ positions were determined by ¹H nuclear magnetic resonance (NMR) analysis (Ragnhild *et al.* 1997). ¹H NMR spectra of O-CMCS were recorded using a Fourier Transform NMR instrument (FT-NMR 400, Bruker, USA). O-CMCS samples were dissolved in D₂O at a concentration of 10 mg/mL, whereas chitosan samples were dissolved in a mixture of D₂O and CD₃COOD (1:99, v/v). The measurement conditions were as follows: 64k data points, an acquisition time of 4.08 s, and 32 scans. The DS was determined by integrating the proton signals corresponding to each position using Top Spin 4.4.0 (Bruker BioSpin, Ettlingen, Germany) software, following Eqs. 1 to 4. Figure 1b represents the resonance of hydrogen atom bonded to C₁ (H-1A, 3.9 ppm), c is the resonance of O-CH₂COOD (H-3', 3.8 ppm), d represents H-6' and H-3' proton resonance (3.3 ppm), whereas g represents the H-2D proton, which is located on the glycosidic ring (2.7 ppm),

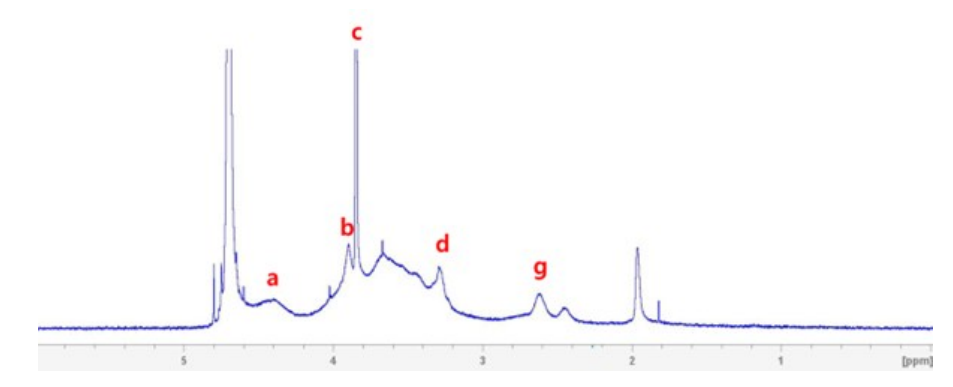


Fig. 1. ¹H NMR spectrum of CMCS 30

$$f_6 = (1/2)(I_d - I_c)/(I_b + I_a) \tag{1}$$

$$f_3 = I_c/(I_b + I_a) \tag{2}$$

$$f_2 = (1/2)I_f/(I_b + I_a) \tag{3}$$

$$F = f_6 + f_6 + f_2 \tag{4}$$

where f_6 , f_3 , and f_2 denote the fractions of carboxymethylation at the 6-O-, 3-O-, and 2-N- positions; F represents the total fraction of carboxymethylation; and I_x (x: b, c, d, g, f) donates the integral value of the hydrogen region corresponding to each location.

Preparation of CMCS-based Aerogels

The samples preparation process is illustrated in Fig. 2. The CMCS was dissolved in distilled water at 2 wt% and stirred at room temperature for 2 h. The CMCS solution was adjusted to pH 10, at which EH exhibited the highest reactivity using 0.5

N NaOH. The EH was then added dropwise to the CMCS solution, and the mixture was stirred at 40 °C for 12 h. The EH concentration was varied from 1 to 7 wt% with respect to the CMCS amount. Treatment conditions were abbreviated with "EH" followed by the percentage; for instance "EH1" means 1% treatment with EH. In the case of CMCS/CNF solutions, CNF was added at concentrations of 0.5, 1, 2, and 3 wt% to the 2 wt% CMCS solution and stirred at room temperature for 1 h. To improve CNF dispersion, ultrasonic treatment was performed using a probe-type ultrasonic processor (VCX-1500, Sonics, USA) at 70% amplitude for 5 min. A total of 5 wt% EH was added to the CMCS/CNF solution under the optimized condition. The solutions were rapidly poured into a silicon mold with a diameter of 5 cm and left at room temperature for 24 h to undergo gelation and promote stable crosslinking. Finally, the gels were frozen in a refrigerator at -80 °C for 2 h. After being completely frozen, the gel samples were freeze-dried for 72 h at -80 °C under a pressure of 2.5 Pa.

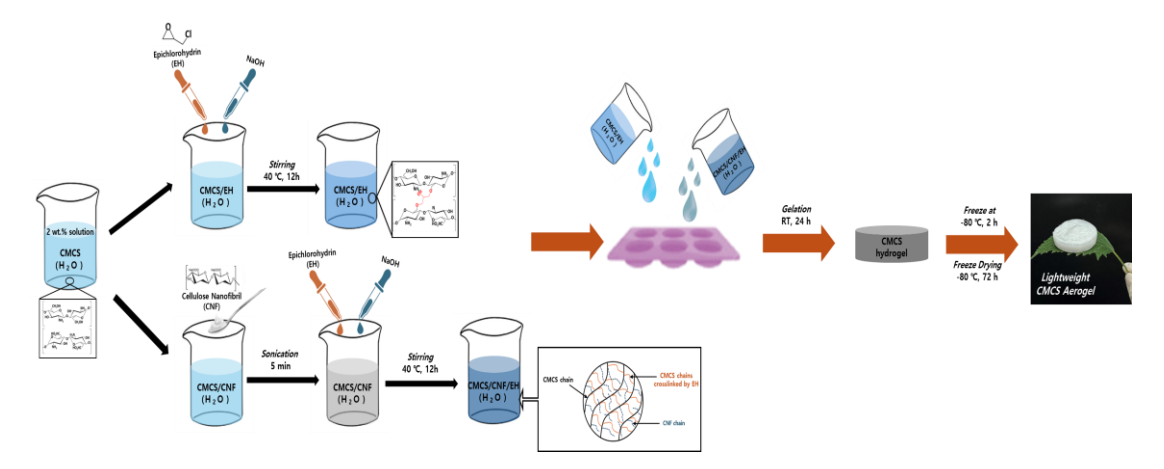


Fig. 2. Schematic illustration of aerogel preparation

Characterization of Aerogels

The apparent density of the prepared aerogel was calculated as follows,

Density
$$(g/cm^3) = \left(\frac{m_0}{\pi(\frac{D}{2})^2 h}\right)$$
 (5)

where m_0 denotes the mass of the aerogels, D represents the aerogel diameter, and h represents the aerogel height. The aerogel porosity was estimated from both the apparent density data and skeletal density as follows,

Porosity (%) =
$$\left[1 - \left(\frac{apparent\ density\ of\ aerogel}{skeletal\ density\ of\ aerogel}\right)\right] \times 100$$
 (6)

where the skeletal density of the CMCS aerogels is 1.528 g/cm³ (Li et al. 2023).

Rheological measurements were performed using stress-controlled rheometer (Hybrid rheometer, HR 20, TA Instrument Co., USA) in a parallel plate setup with a 10 μ m gap. The morphologies of the aerogels were observed using field emission scanning electron microscopy (FE-SEM, JSM-7401F, JEOL, Japan) to observe the pore structure on the surfaces and cross-section of the aerogels with an acceleration voltage of 10 kV. X-ray photoelectron spectroscopy (XPS, ESCALAB250, Thermo Fisher Scientific, USA) was performed to analyze the chemical bonding structure. Compression tests were conducted on cylindrical aerogels with dimensions of $25 \times 25 \times 10$ mm³ using a material testing system (MTS Systems, USA). The tests were conducted at a speed of 12.5 mm/min, and each sample was measured three times to obtain an average value. The engineering stress (σ) was calculated as follows,

Engineering stress
$$(N/m^2) = \frac{F}{A_0}$$
 (7)

where F denotes the normal force and A_0 denotes the area of aerogel.

Validation of Heavy Metal Adsorption

To evaluate the adsorption ability of the prepared aerogels for Pb ions (Pb²⁺), a Pb solution was diluted to a concentration of 100 ppm, and the solution pH was adjusted to 2, 3, 4, 5, and 6 using 0.5 N NaOH. A 30 mL Pb solution was placed in a beaker, and 0.1 g of the aerogels was added. The beaker was then stirred in a shaking incubator at 25 °C and 150 rpm for 12 h. After shaking, the solution was filtered using a glass filter funnel with a pore diameter of 20 to 30 μ m to remove impurities. Subsequently, the equilibrium Pb²⁺ concentration after adsorption process was determined by analyzing the solution *via* inductively coupled plasma atomic emission spectroscopy (IRIS intrepid, Thermo Elemental, USA). The adsorption capacity (q_e) was calculated as follows,

Adsorption capacity
$$(mg/l) = \frac{(C_0 - C_e) \times V}{m}$$
 (8)

where C_0 denotes the initial concentration before adsorption, C_e denotes the equilibrium adsorption concentration, and m represents the aerogel mass.

Adsorption Kinetics Analysis

Adsorption kinetics can be used to evaluate adsorption performance, and the most commonly used kinetic models include the pseudo-first-order (PFO) and pseudo-second-order (PSO) models. Adsorption experiments were conducted at a constant temperature of 25 °C, and q_e values were measured at various time intervals. The adsorption mechanism was analyzed by applying the PFO and PSO kinetic models using Eqs. 9 to 12,

$$pseudo - first - order \ kinetic: q_t = q_e(1 - e^{-K_1 t})$$
 (9)

$$In(q_e - q_t) = In q_e - K_1 t \tag{10}$$

$$pseudo - second - order \ kinetic: q_t = \frac{q_e^2 K_2 t}{1 + q_e K_2 t}$$
 (11)

$$\frac{t}{q_t} = \left(\frac{1}{K_2 q_e^2}\right) + \frac{1}{q_e}t\tag{12}$$

where t represents time, q_e denotes the adsorption volume at equilibrium, q_t denotes the adsorption volume at t, and K_1 and K_2 denote the rate constants of pseudo-first and pseudo-second orders, respectively.

RESULTS AND DISCUSSION

Regioselective Carboxymethylation of CMCS

Depending on the carbon position at which the carboxymethyl group is introduced, various types of CMCS can be synthesized. Among the potential types, CMCS with a carboxymethyl group at the C6 position and an amino group at the C2 position exhibits high solubility and stability across a wide pH range, resulting in diverse surface charge characteristics.

As shown in Fig. 3, regardless of the reaction temperature, carboxyl groups were substituted in the order of $f_6 \ge f_3 > f_2$ because the primary alcohols at the C₆ position are more reactive than the secondary alcohols at the C₃ and C₂ positions (Rinaudo *et al.* 1992). DS increased considerably at temperatures above 20 °C. In particular, CMCS30,

which exhibited the highest DS 1.96, was selected as the optimal sample in this study. This degree of substitution was considered appropriate because it ensured sufficient carboxymethyl substitution to provide water solubility and abundant -COOH functional groups for Pb^{2+} binding, while avoiding excessive substitution that could compromise the polymer backbone and reduce the mechanical stability of the aerogels. When the reaction temperature was above 40 °C, an increase in the value of f_2 and the substitution reaction did not affect f_6 and f_3 .

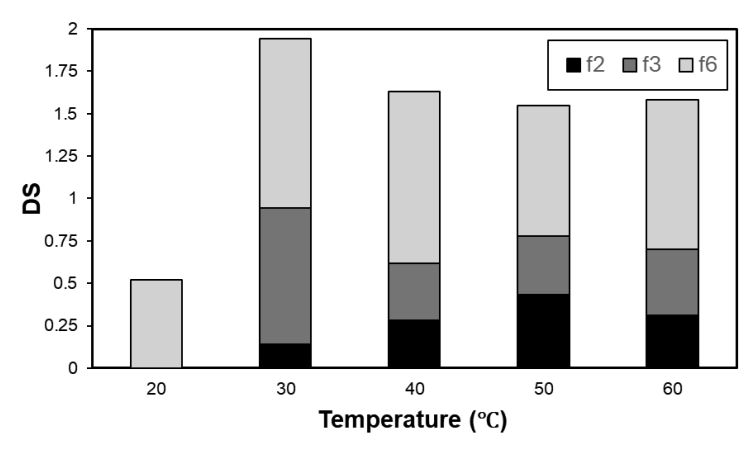


Fig. 3. Degree of substitution (DS) of CMCS at various reaction temperatures

Although the molecular weight of CMCS after carboxymethylation was not directly measured in this study, Du and Hsieh (2008) demonstrated that CMCS maintains excellent solubility when the degree of substitution is sufficiently high (≥0.73), regardless of molecular weight variation. This finding suggests that carboxymethylation enhances functionality without severely compromising the integrity of the polymer backbone. In this study, the viscosity of CMCS solutions was primarily influenced by polymer concentration and degree of substitution, and no processing difficulties were encountered during aerogel preparation. Nevertheless, a detailed molecular weight analysis would provide further insight into the structure–property relationship and is suggested as a direction for future research.

Analysis of Chemical Properties and Structure

Figure 4 shows the attenuated total reflectance infrared (ATR-IR) spectra of CMCS30 and pristine chitosan. The primary peaks of both samples for characterization were at 3300 cm⁻¹ (O-H stretch), 1410 cm⁻¹, 1582 cm⁻¹ (COO- asymmetrical and symmetrical stretch), and 1055 cm⁻¹ (C-O stretch). In the ATR-IR spectrum of pure chitosan, a C=O stretching peak was observed at 1651 cm⁻¹, attributed to residual amide groups from partially deacetylated chitin. In addition, an N-H bending vibration appeared at 1593 cm⁻¹, which is presumed to originate from the acetylated amine groups in the chitosan chains (Huang et al. 2016). In the case of CMCS30, the intensity of the O-H stretching band around 3300 cm⁻¹ significantly increased compared with that of chitosan, indicating enhanced hydrogen bonding due to the introduction of carboxymethyl groups. Compared with the peaks of chitosan, the peaks at 1582 and 1410 cm⁻¹, corresponding to the asymmetric and symmetric stretching of COO⁻ groups, respectively, were noticeably stronger in CMCS30, confirming the successful incorporation of carboxyl groups. A shift and intensity enhancement of the peak near 1055 cm⁻¹, associated with C-O stretching, was also observed, which can be attributed to carboxymethylation occurring predominantly at the C₆ position. These results demonstrate that the carboxymethylation of chitosan was successful (Huang et al. 2016).

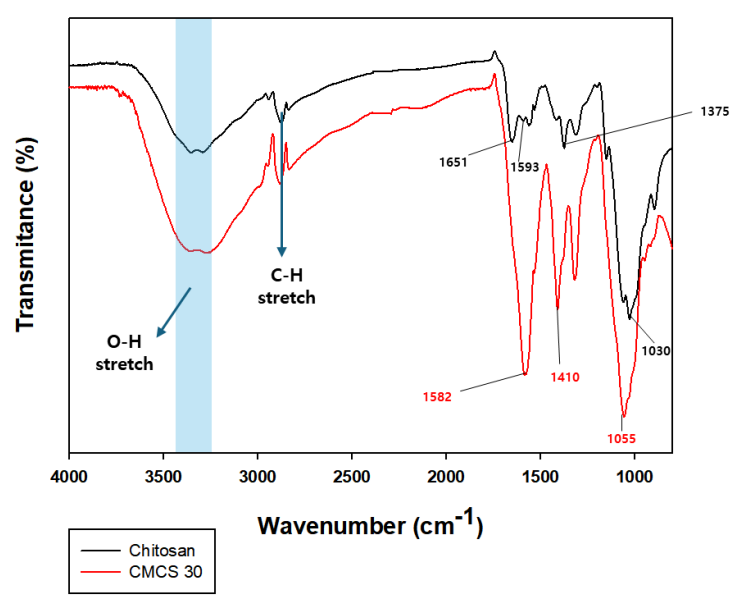


Fig. 4. ATR-IR spectra of chitosan and CMCS30

Figure 5 presents the results of the ¹H NMR spectra of chitosan, CMCSRT, CMCS30, and CMCS50. A peak at 2.0 ppm was observed, corresponding to the -C(O)CH₃ group, which originates from the residual acetyl groups of incompletely deacetylated chitin. In the case of chitosan, an additional signal from the CD₃COOD used as the NMR solvent was also detected (Jaidee et al. 2012). The signals observed at 3.8 to 3.9 ppm indicate hydrogen atoms on the carboxymethyl groups substituted at the C₆ position, confirming successful carboxymethylation. The peak near 2.0 to 2.1 ppm corresponds to the hydrogen at the C₂ position, which is located in proximity to various functional groups such as -NH2, -NHCOCH3, and -NHCH2COO-. This leads to increased sensitivity of the C₂ chemical environment, frequently resulting in peak broadening or slight positional shifts in the spectrum (Cerrutti et al. 2013). The signal intensity at 3.3 ppm was significantly weaker in CMCS30 than in CMCS50, which is consistent with the DS value at the C₂ position (f₂) shown in Fig. 3 (Vaghani *et al.* 2012). This phenomenon can be explained by differences in nucleophilicity and steric hindrance with respect to the reaction temperature. In general, under alkaline conditions, the oxygen atoms of hydroxyl groups are stronger nucleophiles than amine groups. Primary alcohols exhibit high reactivity in carboxymethylation reactions because of their lower steric hindrance than that of amine groups at the C2 position. These compounds enhance the reactivity of C6-OH, thereby making it more favorable for carboxymethylation than the C₂–NH₂ site at low reaction temperatures.

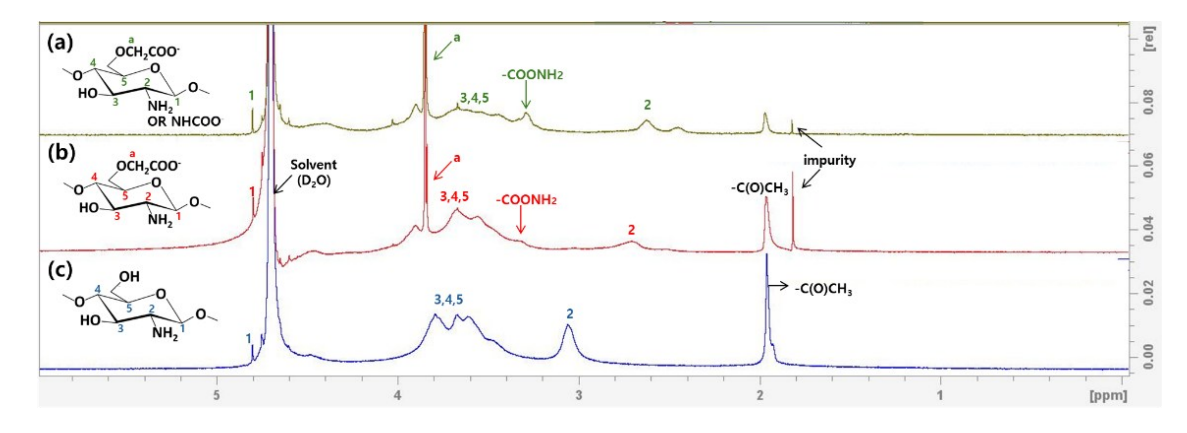


Fig. 5. ¹H NMR spectrum (a: CMCS 50; b: CMCS 30; c: chitosan)

Effects of Crosslinking and CNF on Polymer Network of Aerogels

The viscosities of all CMCS/EH solutions exhibited shear-thinning behavior and increased with increasing EH content (Fig. 6(a)). This result can be attributed to the formation of additional crosslinks between CMCS chains, which enhances intermolecular interactions and restricts the mobility of the CMCS molecular chains. Figure 6(b) shows the measured storage modulus (G') and loss modulus (G''), where G'> G'' indicates solid-like behavior, and G'' > G' indicates liquid-like behavior. In the cases of CMCS and CMCS/EH1, G" exceeded G', demonstrating liquid-like characteristics. In contrast, CMCS/EH3, EH5, and EH7 showed solid-like behavior, with G' being consistently higher than G'' across all frequencies. These results suggest that solutions containing 3 wt% or more EH exhibit enhanced crosslinking, leading to rigid structures and improved elastic properties. Figure 6(c) shows the tan delta (tan δ) values, which are defined as the ratio of G'' to G'. In general, a tan δ value less than 1 indicates a more elastic and rigid polymer structure, whereas a value greater than 1 corresponds to a more viscous and flowable behavior. As the EH content increased, the $\tan \delta$ values decreased, suggesting the formation of a more rigid network due to enhanced crosslinking. The CMCS and CMCS/EH1 samples exhibited tan δ values > 1, whereas the CMCS/EH3, EH5, and EH7 samples exhibited tan δ values < 1.

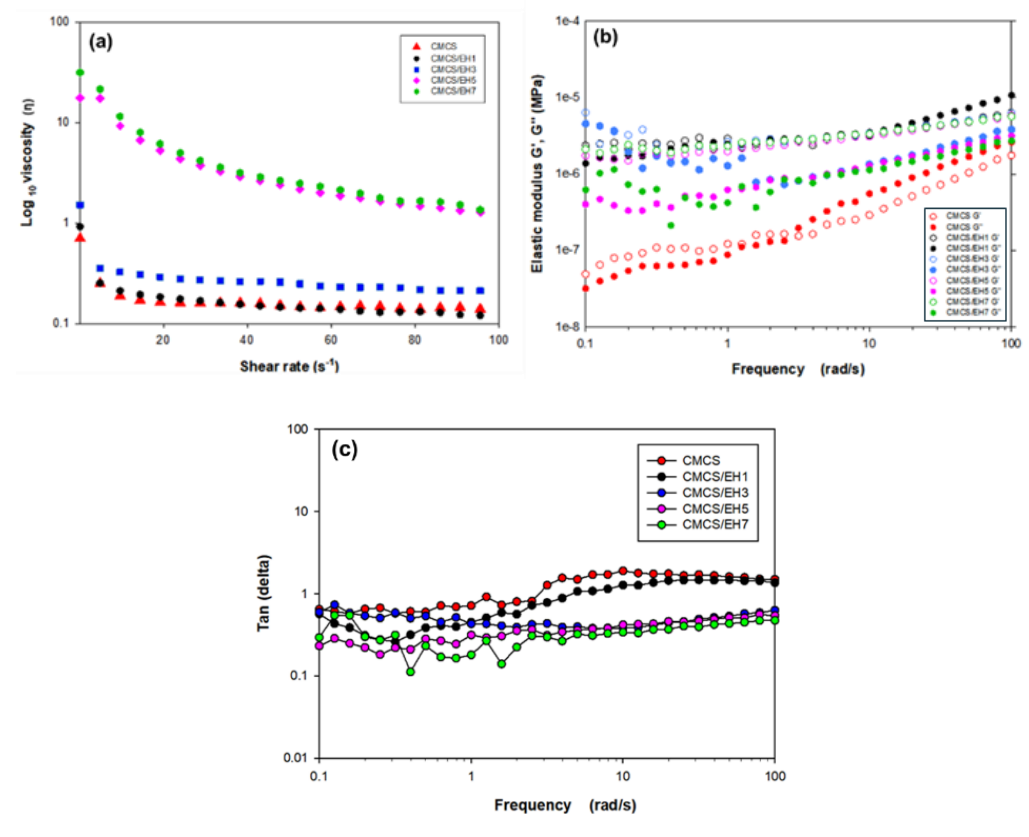


Fig. 6. Rheological behavior of CMCS/EH solutions with different EH concentrations (a: shear viscosity; b: G' and G''; c: tan delta)

The viscosities of all CMCS/CNF solutions also exhibited shear-thinning behavior. However, the viscosity decreased upon the addition of CNFs. This behavior is attributed to electrostatic repulsion between the anionic CNF and CMCS, which weakens the intermolecular interactions between the two polymers. In addition, the protonated amino groups (–NH₃+) and carboxylate groups (–COO⁻) in CMCS and CNF, respectively, exhibit higher affinity for water molecules than for each other, thereby improving the hydration of the polymers and increasing chain mobility within the

solution, which also decreases viscosity (Fig. 7(a)). The CMCS/CNF sample also exhibited solid-like behavior, as shown in Fig. 7(b). The addition of CNFs did not significantly alter the fluid behavior. As shown in Fig. 7(c) regardless of concentration, the CMCS/CNF sample exhibited a $\tan \delta$ value lower than 1, indicating dominant elastic behavior. This trend is consistent with the previously presented viscosity modulus results.

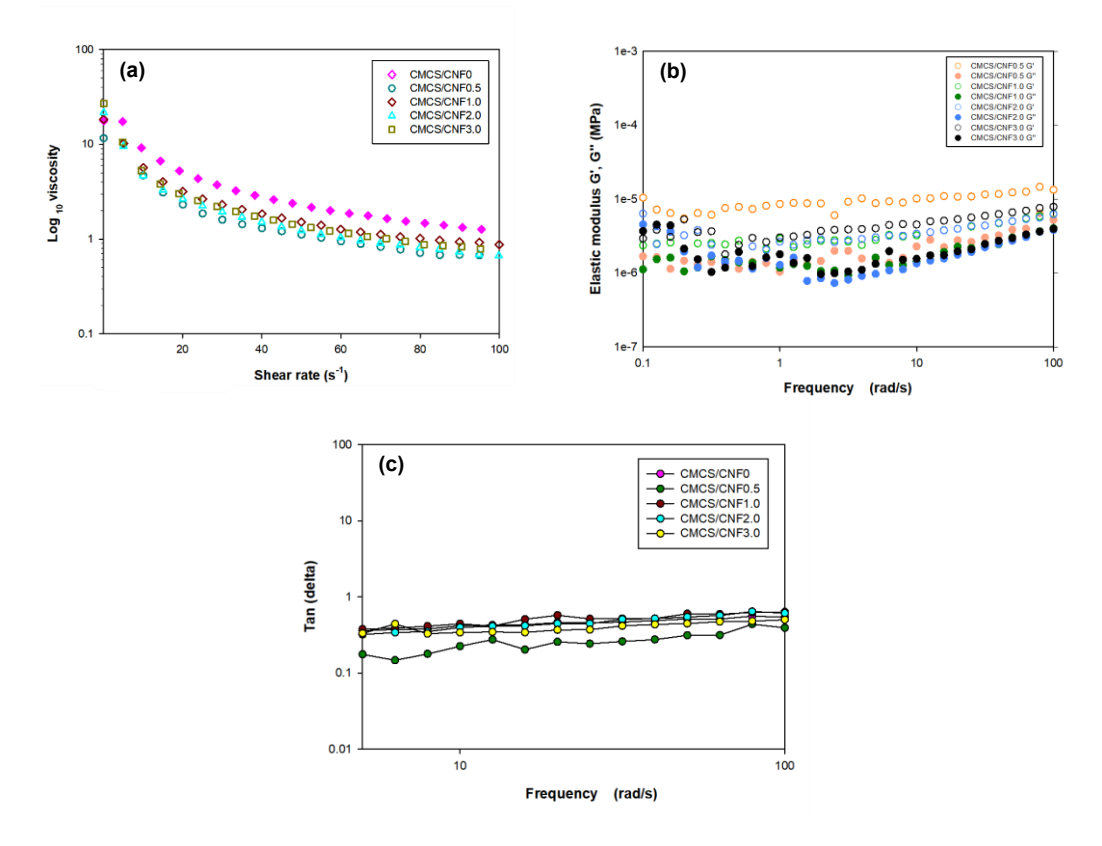


Fig. 7. Rheological behavior of CMCS solutions with different CNF concentrations (a: shear viscosity; b: G' and G''; c: tan delta)

Figure 8 shows the XPS spectra of CMCS, CMCS/EH5, and CMCS/CNF1. The C-C peak (284.7 eV) increased with the addition of EH and CNF, whereas the C-O (C-OH) peak (286 eV) decreased, indicating the formation of chemical bonds between the OH groups of CMCS and EH or CNF. Based on the N1s spectra, the N–H peak (398 to 399 eV) decreased with the addition of EH, suggesting that some amine groups were combined during the crosslinking process. However, the peak intensity increased upon CNF addition due to the enhanced interaction between the -OH and -COOH groups of CNF and EH. Based on the O1s spectra, the C-O-C peak increased with addition, because of the formation of ether bonds between the -OH groups of CMCS and EH. The addition of CNF decreased in the O–H peak but increased the C-O-C peak. This can be attributed to the interaction between the hydroxyl groups of CNFs, EH, and CMCS, facilitating the formation of ether bonds and contributing to the formation of a more robust aerogel structure.

Therefore, the ether linkages formed between CMCS and EH yielded a crosslinked structure, thereby enhancing structural stability (Fig. 9). Furthermore, upon CNFs addition, a more rigid three-dimensional (3D) network was formed through additional ether bond formation among the hydroxyl groups of CNFs, CMCS, and EH, driven by the interpenetrating network of CNFs.

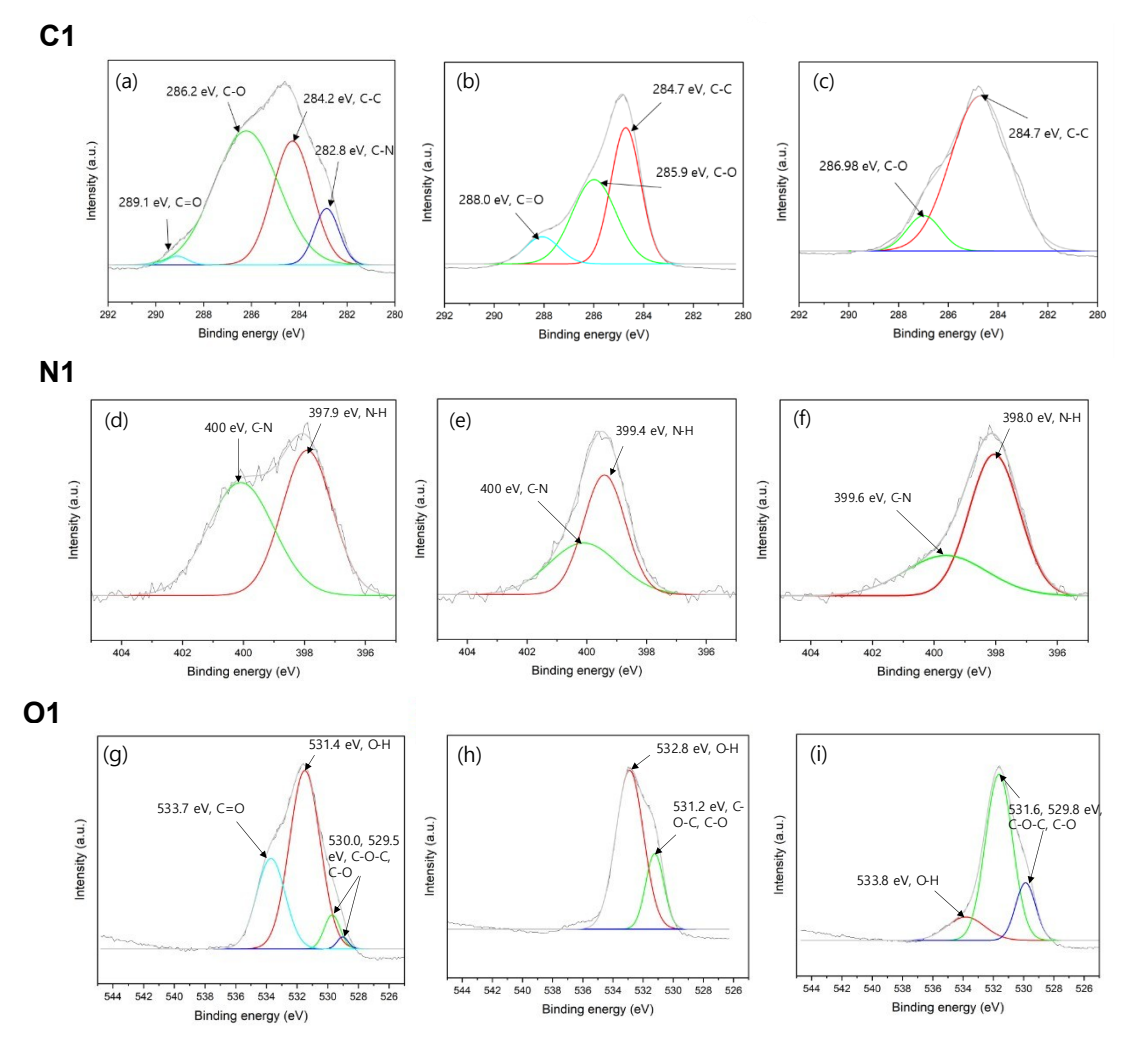


Fig. 8. XPS spectra of CMCS aerogels (a, d, e: CMCS; b, e, h: CMCS/EH5; c, f, i: CMCS/CNF1)

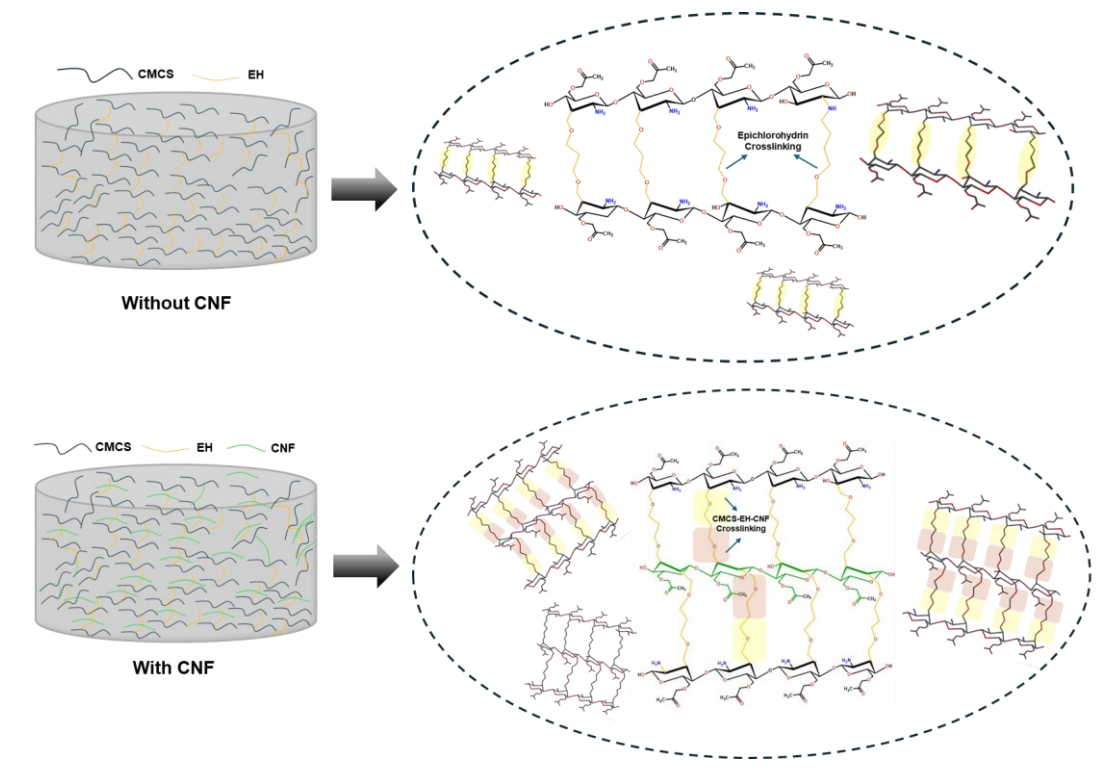


Fig. 9. Component interaction of CMCS/EH/CNF aerogels

Structural Properties of Aerogels

Figure 10 illustrates the effect of EH concentration on the density and porosity of the CMCS aerogels. The densities and porosities of the prepared CMCS aerogels showed that EH decreased aerogels' density but increased the aerogel porosity up to 1 wt%. As the EH content increased beyond 3 wt%, the aerogel density decreased, but the porosity increased. The enhancement of the chemical crosslinking between CMCS and EH led to the formation of a more stable aerogel structure. This resulted in increased porosity and a corresponding decrease in density (Gupta *et al.* 2018).

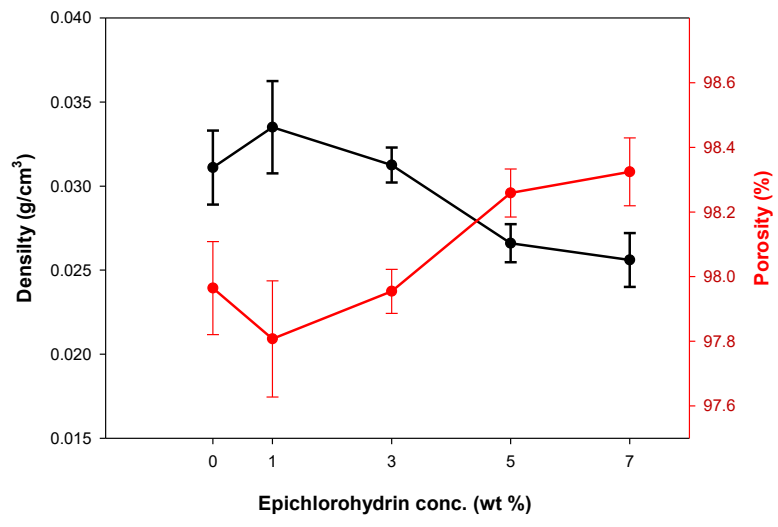


Fig. 10. Effect of EH concentration on density and porosity of CMCS aerogels

The SEM images of the aerogel samples are shown in Figs. 11 and 12. With increasing EH content, the microstructures of the aerogels changed from a disordered, closed structure to a uniform, open porous structure. Aerogels containing more than 3 wt% EH exhibited a honeycomb-like 3D porous structure. This transformation was likely due to the decreased amount of saturated water during gelation as the crosslinker concentration was increased, which promoted the formation of a more stable and interconnected polymer network (Van Nguyen et al. 2022). In the case of EH7, the aerogels exhibited a distinct flake-like morphology. This can be attributed to the strong crosslinking effect of EH, which restricts chain mobility during the drying process, leading to the formation of a compact, plate-like structure (Ko et al. 2020). Figure 12 shows the SEM images of the aerogels containing different CNF concentrations. The incorporation of CNFs led to a more compact aerogel network. For the aerogel CMCS/CNF0.5 condition, CNFs were uniformly dispersed throughout the aerogels structure, forming a thin fibrous sheet-like network. The CMCS/CNF1.0 sample exhibited a significantly thicker fiber network (Fig. 12(b)). However, further increases in CNF loading (2 wt%) resulted in the clogging of surface pores. In addition, the porous structure collapsed, and a lamellar structure was observed. This indicates that higher CNF concentrations promote lateral aggregation, causing CNFs to accumulate between ice crystals, thereby hindering the development of the pore structure (Hult et al. 2001). Thus, the CNF content is directly related to the formation of ice crystals during freeze-drying, which significantly affects the resulting aerogel structure (Thybo et al. 2008).

As shown in Fig. 13(a), ultra-lightweight aerogels were successfully fabricated. Figure 13(b) shows images of the structural maintenance of the aerogels after swelling. The untreated CMCS aerogel rapidly collapses its structure and dissolved into water. Similarly, the aerogel sample with 1 wt% EH exhibited poor structural stability. In

contrast, aerogels containing 3 wt% or more EH successfully maintained their structures even after swelling. Grayscale analysis was performed using the PicMan image processing and analysis software (WaferMasters, Inc., Dublin, CA, USA) and is illustrated in Figs. 13(c), (d). As the EH content increased, the aerogels exhibited a finer and smoother morphological surface. Water molecules crystallize into ice during freezing, and the polymer chains are expelled into the interstitial regions between the growing ice crystals, leading to the formation of aerogel structures. At low crosslinker concentrations, the polymer network lacks sufficient rigidity to resist the directional growth of ice crystals, resulting in irregular porous structures formed along disordered ice crystal growth during freeze-drying. In contrast, higher crosslinker concentrations enhance the robust structure of the polymer matrix, leading to the formation of uniform and smooth porous architectures (Gutiérrez et al. 2008).

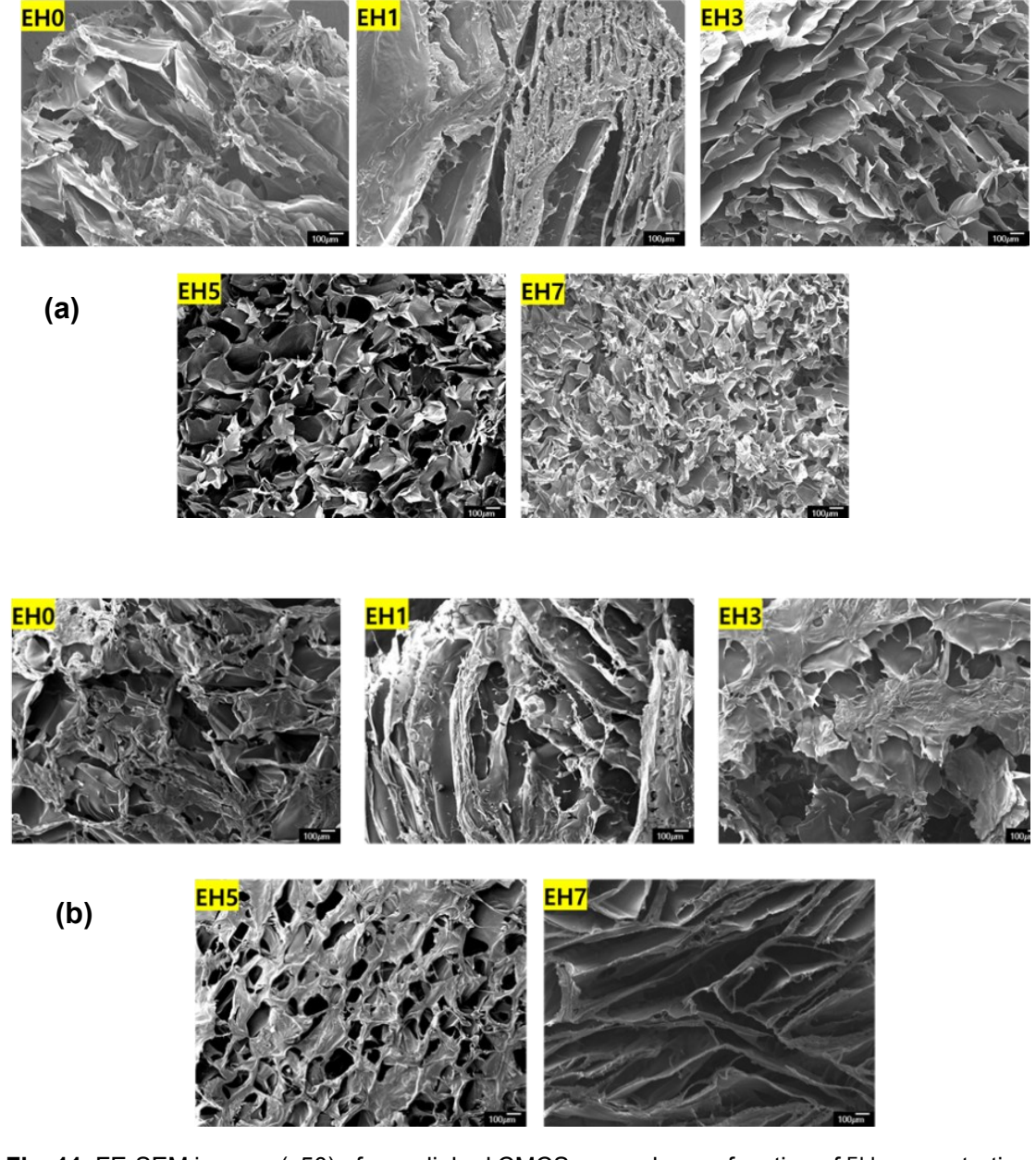


Fig. 11. FE-SEM images (x50) of crosslinked CMCS aerogels as a function of EH concentration (a: cross-sectional images; b: surface images)

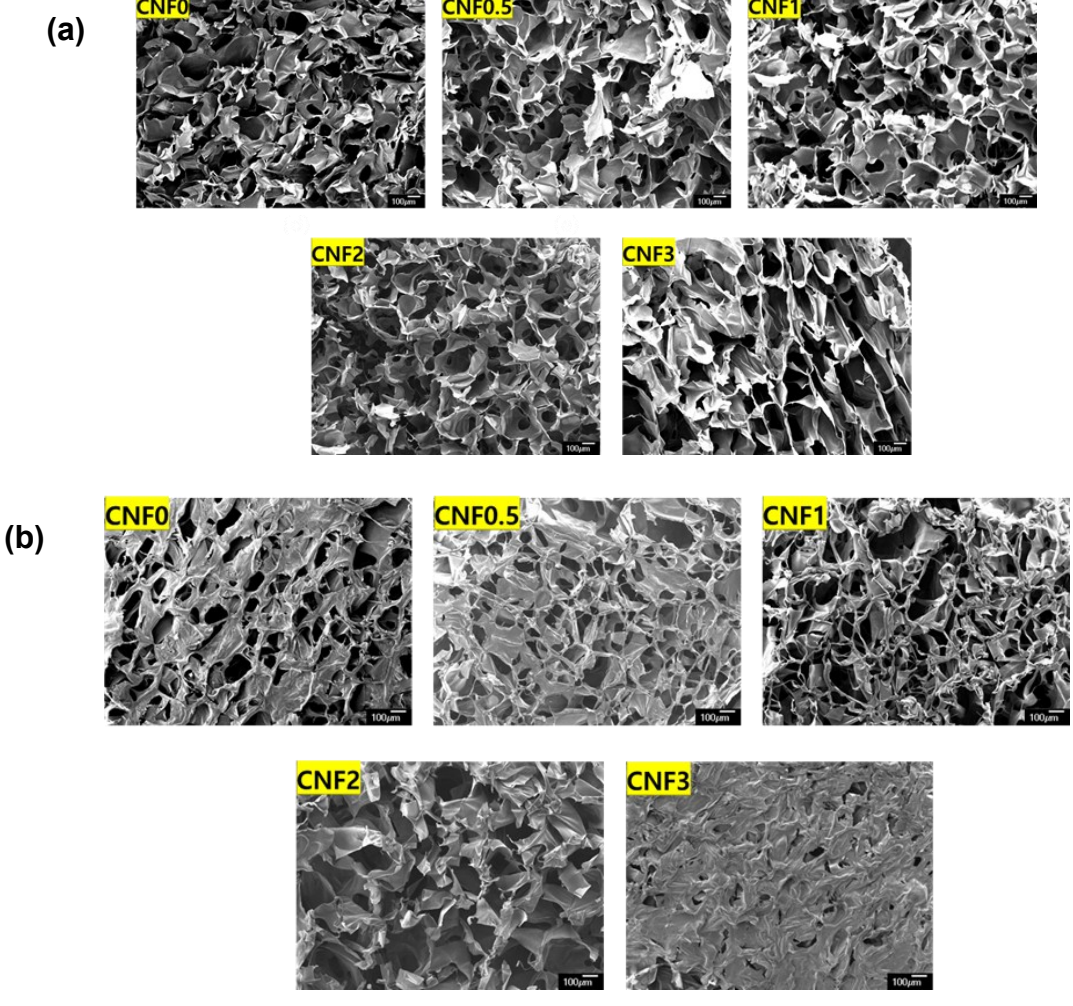


Fig. 12. FE-SEM images (x50) of cross-linked CMCS/EH5 aerogels with 0, 0.5, 1, and 2 wt% CNF loadings (a: cross-sectional images; b: surface images)

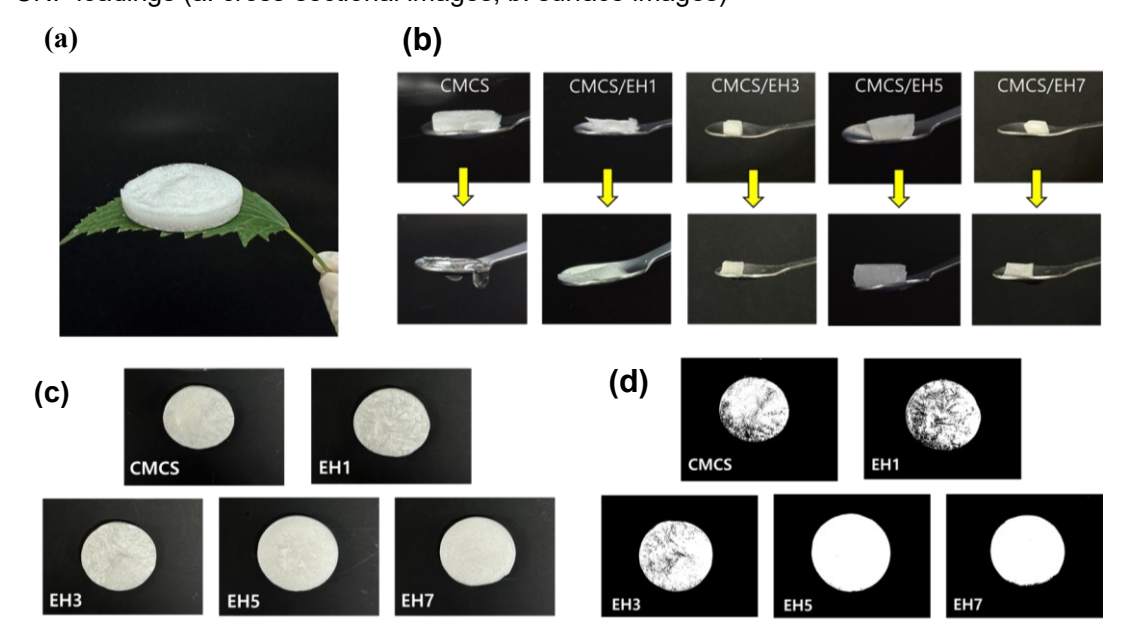
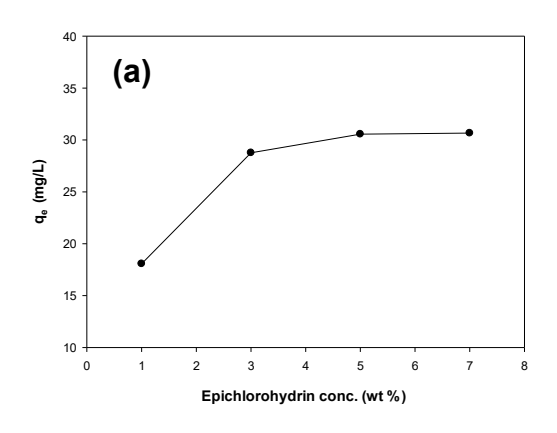


Fig. 13. CMCS aerogel images (a: lightweight CMCS aerogel; b: structural maintenance after swelling; c: aerogels images with 75% grayscale)

Adsorption Performance of Aerogels

The Pb²⁺ adsorption capability of the prepared CMCS aerogels depending on pH is shown in Fig. 14. The carboxyl groups of the CMCS aerogels dissociate at high

pH, leading to negative charges (Borsagli *et al.* 2015). Therefore, electrostatic interactions between carboxyl groups and Pb²⁺ ions occur in the adsorption effect (Akter *et al.* 2021). As the EH content was increased, the adsorption capacity also increased, with aerogels containing 3 wt% or more EH exhibiting adsorption efficiency exceeding 90%. Despite the formation of a dense structure, given that crosslinking primarily occurs *via* hydroxyl groups, many carboxylate groups remain on the aerogel surface, facilitating adsorption. In contrast, the CMCS/EH1 sample exhibited the lowest adsorption capacity (58.1%). This was attributed to formation of a close structure due to shrinkage. Therefore, based on its superior adsorption performance, CMCS/EH5 was selected as the optimal sample and used in subsequent experiments. To enhance adsorption performance, aerogels should possess a stable 3D structure with numerous small and uniform pores (She *et al.* 2018).



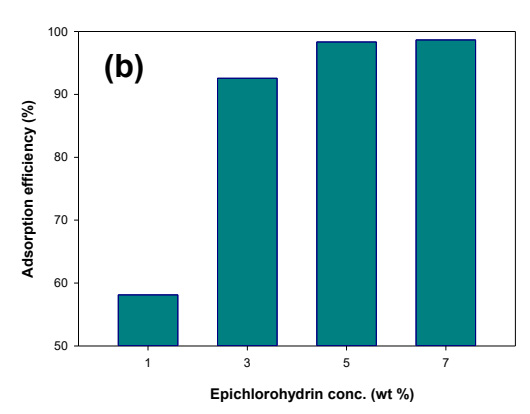


Fig. 14. Adsorption performance of CMCS/EH aerogels at pH 6 (a: adsorption capacity; b: adsorption efficiency)

Table 3 presents the Pb²⁺ adsorption test results for the aerogels at different pH levels. In the pH range of 3 to 6, the adsorption efficiency was 99%, whereas at pH 2, the adsorption efficiency was reduced to 3% to 18%. This result can be attributed to the pH-dependent characteristics of the CMCS/CNF aerogels. At higher pH levels, -COOH deprotonates and forms negatively charged -COO-, which binds with Pb²⁺ ions (Borsagli *et al.* 2015). At lower pH, protonation of -COOH and NH₃⁺ reduces the adsorption of cationic heavy metal ions (Ramanery *et al.* 2014). At pH 2, the adsorption efficiency increased with increasing CNF content. During the adsorption process, an increase in CNF content raises the carboxyl group in the aerogels, generating competing charged ions, such as Na⁺ and H⁺ (Maurya *et al.* 2006), which ion hinder Pb²⁺ adsorption. Therefore, excessive CNF content hinders heavy metal ion adsorption.

Table 3. Adsorption Data of CMCS/CNF Aerogels at Different pH Levels

	pH2		pH3		pH4		pH5		pH6	
	Adsorption		Adsorption	q e	Adsorption		Adsorption	q e	Adsorption	
Sample	efficiency	(mg/g)	efficiency	(mg/g)	efficiency	(mg/g)	efficiency	(mg/g)	efficiency	(mg/
	(%)		(%)		(%)		(%)	(9,9)	(%)	g)
CNF 0	3.04	26.66	99.60	32.12	99.69	31.97	99.45	31.48	98.34	30.56
CNF 0.5	9.90	28.91	99.72	32.16	99.78	32.00	99.77	31.58	99.59	31.02
CNF 1	17.82	32.12	97.92	31.66	99.38	31.87	99.10	31.37	99.20	31.87
CNF 2	18.49	33.32	99.31	32.03	99.58	31.94	99.62	31.53	99.10	31.83
CNF 3	18.68	33.68	98.98	31.92	99.51	31.91	99.47	31.48	99.37	31.94

Taken together, the analysis of Pb²⁺ adsorption as a function of CNF content revealed that the overall adsorption capacity did not increase further beyond 1 wt%. This behavior can be attributed to partial agglomeration of CNFs at higher loadings, which may block or reduce the accessibility of –COOH active sites on CMCS. In addition, excessive CNF incorporation could lead to a denser microstructure and restricted pore accessibility, thereby limiting Pb²⁺ diffusion into the aerogel network. These findings suggest that 1 wt% CNF represents an optimal balance between mechanical reinforcement and adsorption efficiency.

Figure 15 and Table 4 present the adsorption kinetics of Pb²⁺ onto the CMCS aerogels and evaluated using the pseudo-first-order (PFO) and pseudo-second-order (PSO) models. The R² values for both samples, when using the PSO model, reached 0.9998 and 0.9995, respectively. Though the PSO model is not based on a valid derivation, it has been found that good fits of data to the PSO model are consistent with diffusion into a network of tiny pores as the rate-limiting step in adsorption (Hubbe *et al.* 2019).

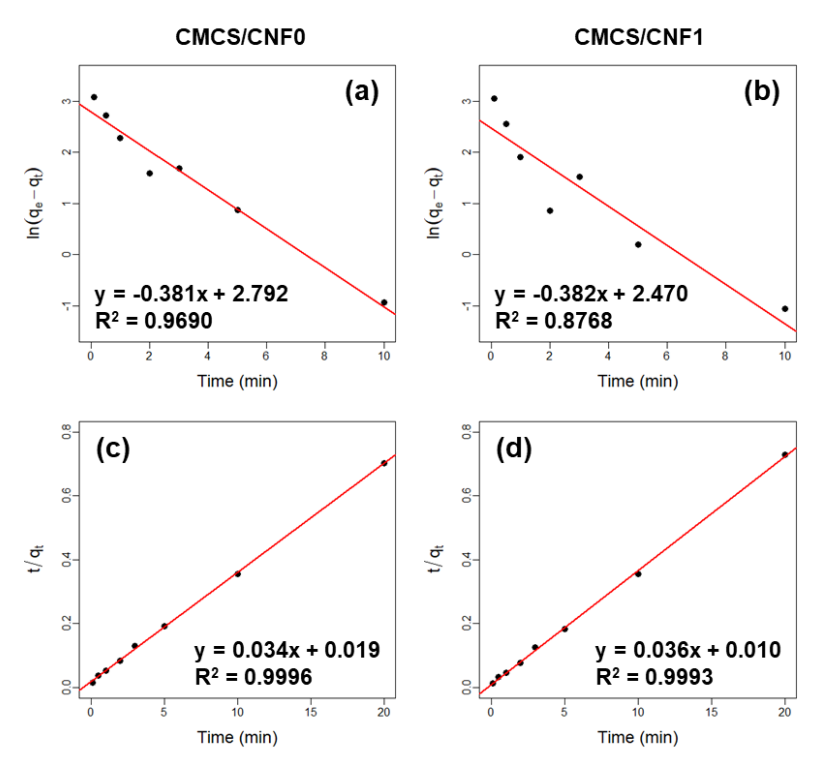


Fig. 15. Adsorption kinetic plots (a, b : PFO kinetic model; c, d : PSO kinetic model)

Table 4. Kinetic Parameters for Adsorption of CMCS/CNF Aerogels

Kinetic Model	Kinetic Parameter	CMCS/CNF 0	CMCS/CNF 1.0
PFO	K₁ (1/min)	0.381	0.382
	<i>q</i> e (mg/g)	16.31	11.83
	R^2	0.9690	0.8768
PSO	K ₂ (g/mg min)	0.062	0.130
	<i>q</i> _e (mg/g)	29.24	28.01
	R ²	0.9996	0.9993

Mechanical Property Measurements of CMCS/CNF Aerogels

The compressive strength of the aerogels depended on the matrix microstructure. Figure 17 shows the compressive strength of the aerogels. The strength of the aerogels with CNF loading was higher than that of the aerogels without CNF loading. This

improvement can be attributed to the formation of a more compact matrix microstructure by CNF addition (Fig. 12) (Wang et al. 2020). The aerogel samples with 1 wt% CNF loading exhibited the highest strength enhancement (240 kPa), representing a 42% improvement over the aerogels without CNF loading. As the CNF content increased to 2 wt%, the compression strength decreased; however, it was still higher than the strength of the aerogels without CNF loading.

In addition to the structural and adsorption performance, it is noteworthy that the preparation of CMCS/CNF aerogels relies on simple aqueous-based reactions and freeze-drying without the need for costly reagents or specialized equipment. Compared with silica- or synthetic polymer-based aerogels that typically require complex sol—gel chemistry and supercritical drying, the present system is relatively time- and cost-effective, which enhances its practical applicability. Moreover, a comprehensive life-cycle and cost analysis in comparison with conventional aerogels would be a meaningful direction for future research.

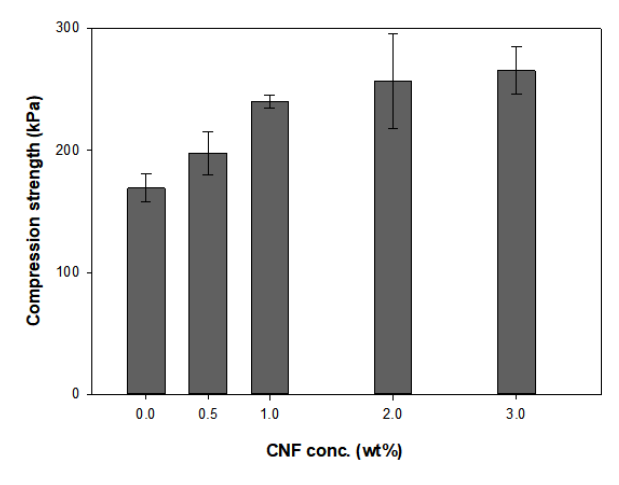


Fig. 16. Compression strength of aerogels with different CNF concentrations

Comparison of the Aerogels with Other Reported Adsorbents

A comparison of the Pb^{2+} adsorption performance of the fabricated CMCS/CNF aerogels with that of other previously reported adsorbents is presented in Table 5. The CMCS/CNF aerogel exhibits a comparable or higher adsorption capacity (~32 mg/g) than other adsorbents, confirming its effectiveness. These results indicate that the developed aerogel is a promising and sustainable material for Pb^{2+} removal from aqueous solutions.

Table 5. Comparison of maximum Pb²⁺ adsorption capacities of CMCS/CNF aerogels and reported adsorbents.

Adsorbents	q _e (mg/g)	References
Chitosan/sand	12.32	Wan <i>et al.</i> (2010)
Chitosan/cellulose	26.31	Sun <i>et al.</i> (2009)
Carboxymethylated cellulose	24.59	Chen et al. (2008)
Fe ₃ O ₄ /CNTs	21.55	Elmi <i>et al.</i> (2017)
Carboxymethyl chitosan/cellulose nanofibril composite aerogel (CMCS/CNF 1.0)	31.87	This work

From a reusability perspective, although adsorption—desorption experiments were not performed in this study, previous reports have demonstrated that Pb²⁺ ions adsorbed onto polysaccharide-based materials can be effectively eluted using dilute acids (e.g., HCl) or chelating agents such as EDTA, thereby enabling multiple regeneration cycles (Bayuo et al. 2020; Anitha et al. 2016). Given the stable crosslinked

network structure of CMCS/CNF aerogels, it is reasonable to expect that similar regeneration strategies could be applied, allowing these aerogels to be reused in practical applications. Future research should therefore focus on systematic adsorption—desorption studies to verify the long-term reusability and structural stability of the developed aerogels.

CONCLUSIONS

- 1. The prepared carboxymethyl chitosan (CMCS) was soluble in aqueous media and used as a heavy metal adsorption material.
- 2. The CMCS composite aerogels with uniform 3D network microstructures were successfully prepared by freeze-drying and crosslinking methods. CMCS, epichlorohydrin (EH), and cellulose nanofibers (CNF) were mixed uniformly in water. The addition of 3 wt% or more EH formed uniform 3D porous aerogel network structures.
- 3. Pb²⁺ adsorption capacity increased from 58% at 1% EH (EH1) to 98% at EH5 due to the formation of stable structures.
- 4. The addition of cellulose nanofibers (CNFs) resulted in the formation of a dense composite aerogel structure. The mechanical strength was enhanced 42% with the addition of 1 wt% CNF loading compared to the composite aerogels without CNF.

ACKNOWLEDGMENTS

This work was supported by the Ministry of Culture, Sports and Tourism of the Republic of Korea and a National Research Foundation of Korea (NRF) grant funded by the Korean government (NRF-2022M3C1C5A02094347).

REFERENCES CITED

- Abdel-Halim, E. S., and Al-Deyab, S. S. (2011). "Removal of heavy metals from their aqueous solutions through adsorption onto natural polymers," *Carbohydrate Polymers* 84(1), 454-458. DOI: 10.1016/j.carbpol.2010.12.001
- Akter, M., Bhattacharjee, M., Dhar, A. K., Rahman, F. B. A., Haque, S., Rashid, T. U., and Kabir, S. F. (2021). "Cellulose-based hydrogels for wastewater treatment: A concise review," *Gels* 7(1), article 30. DOI: 10.3390/gels7010030
- Anitha, T., Kumar, P. S., Kumar, K. S., Sriram, K., and Ahmed, J. F. (2016). "Biosorption of lead (II) ions onto nano-sized chitosan particle blended polyvinyl alcohol (PVA): adsorption isotherms, kinetics and equilibrium studies," *Desalination and Water Treatment* 57(29), 13711-13721. DOI: 10.1080/19443994.2015.1061951
- Bayuo, J., Abukari, M. A., and Pelig-Ba, K. B. (2020). "Desorption of chromium (VI) and lead (II) ions and regeneration of the exhausted adsorbent," *Appl. Water Sci.* 10, 1-6. DOI: 10.1007/s13201-020-01250-y
- Bekchanov, D., Mukhamediev, M., Yarmanov, S., Lieberzeit, P., and Mujahid, A. (2024). "Functionalizing natural polymers to develop green adsorbents for wastewater treatment applications," *Carbohydrate Polymers* 323, Article ID 121397. DOI: 10.1016/j.carbpol.2023.121397

- Bhattarai, N., Gunn, J., and Zhang, M. (2010). "Chitosan-based hydrogels for controlled, localized drug delivery," *Advanced Drug Delivery Reviews* 62(1), 83-99. DOI: 10.1016/j.addr.2009.07.019
- Borsagli, F. G. M., Mansur, A. A., Chagas, P., Oliveira, L. C., and Mansur, H. S. (2015). "O-carboxymethyl functionalization of chitosan: Complexation and adsorption of Cd (II) and Cr (VI) as heavy metal pollutant ions," *Reactive and Functional Polymers* 97, 37-47. DOI: 10.1016/j.reactfunctpolym.2015.10.005
- Chen, S. Y., Zou, Y., Yan, Z. Y., Shen, W., Shi, S. K., and Zhang, X. (2008). "Carboxymethylated-bacterial cellulose for copper and lead ion removal," *Journal of Hazardous Materials* 161, 1355-1359. DOI: 10.1016/j.jhazmat.2008.04.098
- Chen, X. G., and Park, H. J. (2003). "Chemical characteristics of O-carboxymethyl chitosans related to the preparation conditions," *Carbohydrate Polymers* 53(4), 355-359. DOI: 10.1016/s0144-8617(03)00051-1
- Du, J., and Hsieh, Y.-L. (2008). "Nanofibrous membranes from aqueous electrospinning of carboxymethyl chitosan," *Nanotechnology* 19(12), 125707. DOI: 10.1088/0957-4484/19/12/125707.
- Duruibe, J. O., Ogwuegbu, M. O. C., and Egwurugwu, J. N. (2007). "Heavy metal pollution and human biotoxic effects," *International Journal of Physical Sciences* 2(5), 112-118.
- Erosa, M. D., Medina, T. S., Mendoza, R. N., Rodriguez, M. A., and Guibal, E. (2001). "Cadmium sorption on chitosan sorbents: Kinetic and equilibrium studies," *Hydrometallurgy* 61(3), 157-167. DOI: 10.1016/s0304-386x(01)00166-9
- Esmaeili, Z., Izadyar, S., Hamzeh, Y., and Abdulkhani, A. (2021). "Preparation and characterization of highly porous cellulose nanofibrils/chitosan aerogel for acid blue 93 adsorption: Kinetics, isotherms, and thermodynamics analysis," *Journal of Chemical & Engineering Data* 66(2), 1068-1080. DOI: 10.1021/acs.jced.0c00872
- Goel, J., Kadirvelu, K., Rajagopal, C., and Garg, V. K. (2005). "Investigation of adsorption of lead, mercury and nickel from aqueous solutions onto carbon aerogel," *Journal of Chemical Technology & Biotechnology: International Research in Process, Environmental & Clean Technology* 80(4), 469-476. DOI: 10.1002/jctb.1212
- Gu, F., Geng, J., Li, M., Chang, J., and Cui, Y. (2019). "Synthesis of chitosan—lignosulfonate composite as an adsorbent for dyes and metal ions removal from wastewater," *ACS Omega* 4(25), 21421-21430. DOI: 10.1021/acsomega.9b03128
- Gupta, P., Singh, B., Agrawal, A. K., and Maji, P. K. (2018). "Low density and high strength nanofibrillated cellulose aerogel for thermal insulation application," *Materials & Design* 158, 224-236. DOI: 10.1016/j.matdes.2018.08.031
- Gutiérrez, M. C., Ferrer, M. L., and del Monte, F. (2008). "Ice-templated materials: Sophisticated structures exhibiting enhanced functionalities obtained after unidirectional freezing and ice-segregation-induced self-assembly," *Chemistry of Materials* 20(3), 634-648. DOI: 10.1021/cm702028z
- Hjerde, R. J. N., Vårum, K. M., Grasdalen, H., Tokura, S., and Smidsrød, O. (1997). "Chemical composition of O-(carboxymethyl)-chitins in relation to lysozyme degradation rates," *Carbohydrate Polymers* 34(3), 131-139. DOI: 10.1016/s0144-8617(97)00113-6
- Huang, Y. C., and Kuo, T. H. (2016). "O-carboxymethyl chitosan/fucoidan nanoparticles increase cellular curcumin uptake," *Food Hydrocolloids* 53, 261-269. DOI: 10.1016/j.foodhyd.2015.02.006
- Huang, Y. C., and Yang, Y. T. (2016). "Effect of basic fibroblast growth factor released from chitosan–fucoidan nanoparticles on neurite extension," *Journal of Tissue Engineering and Regenerative Medicine* 10(5), 418-427. DOI: 10.1002/term.1752

- Hubbe, M. A., Azizian, S., and Douven, S. (2019). "Implications of apparent pseudo-second-order adsorption kinetics onto cellulosic materials. A review," *BioResources* 14(3), 7582-7626. DOI: 10.15376/biores.14.3.7582-7626
- Hult, E. L., Larsson, P. T., and Iversen, T. (2001). "Cellulose fibril aggregation An inherent property of kraft pulps," *Polymer* 42(8), 3309-3314. DOI: 10.1016/s0032-3861(00)00774-6
- Jaidee, A., Rachtanapun, P., and Luangkamin, S. (2012). "1H-NMR analysis of degree of substitution in N, O-carboxymethyl chitosans from various chitosan sources and types," *Advanced Materials Research* 506, 158-161. DOI: 10.4028/www.scientific.net/amr.506.158
- Jawad, A. H., and Nawi, M. A. (2012). "Characterizations of the photocatalytically-oxidized cross-linked chitosan-glutaraldehyde and its application as a sub-layer in the TiO₂/CS-GLA bilayer photocatalyst system," *Journal of Polymers and the Environment* 20, 817-829. DOI: 10.1007/s10924-012-0434-5
- Jawad, A. H., Mubarak, N. S. A., and Sabar, S. (2019). "Adsorption and mechanism study for reactive red 120 dye removal by cross-linked chitosan-epichlorohydrin biobeads," *Desalination and Water Treatment* 164, 378-387. DOI: 10.5004/dwt.2019.24438
- Ko, E., and Kim, H. (2020). "Preparation of chitosan aerogel crosslinked in chemical and ionical ways by non-acid condition for wound dressing," *International Journal of Biological Macromolecules* 164, 2177-2185. DOI: 10.1016/j.ijbiomac.2020.08.008
- Li, A., Lin, R., Lin, C., He, B., Zheng, T., Lu, L., and Cao, Y. (2016). "An environment-friendly and multi-functional absorbent from chitosan for organic pollutants and heavy metal ion," *Carbohydrate Polymers* 148, 272-280. DOI: 10.1016/j.carbpol.2016.04.070
- Li, T. T., Zang, K., Wang, X., Lou, C. W., and Lin, J. H. (2023). "Zinc borate nanoparticle-loaded carboxymethyl chitosan aerogels for flame retardancy and acoustic absorption," *ACS Applied Nano Materials* 6(21), 20149-20160. DOI: 10.1021/acsanm.3c03918
- Maurya, N. S., Mittal, A. K., Cornel, P., and Rother, E. (2006). "Biosorption of dyes using dead macro fungi: Effect of dye structure, ionic strength and pH," *Bioresource Technology* 97(3), 512-521. DOI: 10.1016/j.biortech.2005.02.045
- Mi, F. L., Shyu, S. S., Lee, S. T., and Wong, T. B. (1999). "Kinetic study of chitosantripolyphosphate complex reaction and acid-resistive properties of the chitosantripolyphosphate gel beads prepared by in-liquid curing method," *Journal of Polymer Science Part B: Polymer Physics* 37(14), 1551-1564. DOI: 10.1002/(sici)1099-0488(19990715)37:14<1551::aid-polb1>3.3.co;2-8
- Mo, L., Zhang, S., Qi, F., and Huang, A. (2022). "Highly stable cellulose nanofiber/polyacrylamide aerogel via in-situ physical/chemical double crosslinking for highly efficient Cu (II) ions removal," *International Journal of Biological Macromolecules* 209, 1922-1932. DOI: 10.1016/j.ijbiomac.2022.04.167
- Ngah, W. W., Ab Ghani, S., and Kamari, A. (2005). "Adsorption behaviour of Fe (II) and Fe (III) ions in aqueous solution on chitosan and cross-linked chitosan beads," *Bioresource Technology* 96(4), 443-450. DOI: 10.1016/j.biortech.2004.05.022
- Özacar, M., Şengil, İ. A., and Türkmenler, H. (2008). "Equilibrium and kinetic data, and adsorption mechanism for adsorption of lead onto valonia tannin resin," *Chemical Engineering Journal* 143(1-3), 32-42. DOI: 10.1016/j.cej.2007.12.005
- Ramanery, F. P., Mansur, A. A., Borsagli, F. G., and Mansur, H. S. (2014). "Green and facile synthesis of water-soluble ZnS quantum dots nanohybrids using chitosan derivative ligands," *Journal of Nanoparticle Research* 16, 1-14. DOI: 10.1007/s11051-014-2504-1

- Rinaudo, M., Le Dung, P., Gey, C., and Milas, M. (1992). "Substituent distribution on O, N-carboxymethylchitosans by 1H and 13C NMR," *International J. Biological Macromolecules* 14(3), 122-128. DOI: 10.1016/s0141-8130(05)80001-7
- Rinaudo, M., Pavlov, G., and Desbrieres, J. (1999). "Influence of acetic acid concentration on the solubilization of chitosan," *Polymer* 40(25), 7029-7032. DOI: 10.1016/s0032-3861(99)00056-7
- She, J., Tian, C., Wu, Y., Li, X., Luo, S., Qing, Y., and Jiang, Z. (2018). "Cellulose nanofibrils aerogel cross-linked by poly (vinyl alcohol) and acrylic acid for efficient and recycled adsorption with heavy metal ions," *Journal of Nanoscience and Nanotechnology* 18(6), 4167-4175. DOI: 10.1166/jnn.2018.15264
- Shrestha, R., Ban, S., Devkota, S., Sharma, S., Joshi, R., Tiwari, A. P., Kim, H. Y., and Joshi, M. K. (2021). "Technological trends in heavy metals removal from industrial wastewater: A review," *Journal of Environmental Chemical Engineering* 9(4), article 105688. DOI: 10.1016/j.jece.2021.105688
- Sorlier, P., Denuzière, A., Viton, C., and Domard, A. (2001). "Relation between the degree of acetylation and the electrostatic properties of chitin and chitosan," *Biomacromolecules* 2(3), 765-772. DOI: 10.1021/bm015531+
- Sun Sheng Ling, S. S., Wang Li, W. L., and Wang Ai Qin, W. A. (2006). "Adsorption properties of crosslinked carboxymethyl-chitosan resin with Pb (II) as template ions," *Journal of Hazardous Materials* 136(3), 930-937.
- Sun, X. Q., Peng, B., Jing, Y., Chen, J., and Li, D. Q. (2009). "Chitosan(chitin)/ cellulose composite biosorbents prepared using ionic liquid for heavy metal ions adsorption," *Separations*, 55, 2062–2069 DOI: 10.1002/aic.11797
- Thybo, P., Hovgaard, L., Andersen, S. K., and Lindeløv, J. S. (2008). "Droplet size measurements for spray dryer scale-up," *Pharmaceutical Development and Technology* 13(2), 93-104. DOI: 10.1080/10837450701830957
- Vaghani, S. S., Patel, M. M., and Satish, C. S. (2012). "Synthesis and characterization of pH-sensitive hydrogel composed of carboxymethyl chitosan for colon targeted delivery of ornidazole," *Carbohydrate Research* 347(1), 76-82. DOI: 10.1016/j.carres.2011.04.048
- Van Nguyen, T. T., Yang, G. X., Phan, A. N., Nguyen, T., Ho, T. G. T., Nguyen, S. T., and Phuong, H. H. K. (2022). "Insights into the effects of synthesis techniques and crosslinking agents on the characteristics of cellulosic aerogels from water hyacinth," *RSC Advances* 12(30), 19225-19231. DOI: 10.1039/d2ra02944h
- Wan Ngah, W. S., Ariff, N. F. M., and Hanafiah, M. A. K. M. (2010). "Preparation, characterization, and environmental application of crosslinked chitosan-coated bentonite for tartrazine adsorption from aqueous solutions," *Water, Air and Soil Pollution* 206, 225-236. DOI: 10.1016/j.carbpol.2010.11.004
- Wang, Z., Zhu, W., Huang, R., Zhang, Y., Jia, C., Zhao, H., and Xue, Y. (2020). "Fabrication and characterization of cellulose nanofiber aerogels prepared *via* two different drying techniques," *Polymers* 12(11), article 2583. DOI: 10.3390/polym12112583
- Wu, F. C., Tseng, R. L., and Juang, R. S. (2010). "A review and experimental verification of using chitosan and its derivatives as adsorbents for selected heavy metals," *Journal of Environmental Management* 91(4), 798-806. DOI: 10.1016/j.jenvman.2009.10.018
- Yano, H., Omura, H., Honma, Y., Okumura, H., Sano, H., and Nakatsubo, F. (2018). "Designing cellulose nanofiber surface for high density polyethylene reinforcement," *Cellulose* 25, 3351-3362. DOI: 10.1007/s10570-018-1787-2
- Yu, J., Zhu, S., Chen, P., Zhu, G. T., Jiang, X., and Di, S. (2019). "Adsorption behavior and mechanism of Pb (II) on a novel and effective porphyrin-based

- magnetic nanocomposite," *Applied Surface Science* 484, 124-134. DOI: 10.1016/j.apsusc.2019.04.075
- Zając, A., Sąsiadek, W., Dymińska, L., Ropuszyńska-Robak, P., Hanuza, J., Ptak, M., and Skrzypczak, K. (2023). "Chitosan and its carboxymethyl-based membranes produced by crosslinking with magnesium phytate," *Molecules* 28(16), article 5987. DOI: 10.3390/molecules28165987
- Zhao, S., Zhang, X., Zhu, D., Zhang, K., Wei, G., and Su, Z. (2023). "Regulating ordered structure and multi-functions of zeolite aerogels for solar steam generation and heavy metal ion adsorption," *Separation and Purification Technology* 324, article 124588. DOI: 10.1016/j.seppur.2023.124588

Article submitted: July 1, 2025; Peer review completed: August 1, 2025; Revised version received and accepted: September 24, 2025; Published: October 23, 2025. DOI: 10.15376/biores.20.4.10618-10639